High-speed 3D imaging based on structured illumination and electrically tunable lens

Dongping Wang (王东平)[1,2], Yunlong Meng (孟云龙)[1,2], Dihan Chen (陈頓瀚)[1,2], Yeung Yam (任 揚)[1,], and Shih-Chi Chen (陳世祈)[1,2,*]**

[1]*Department of Mechanical and Automation Engineering, The Chinese University of Hong Kong, Shatin, Hong Kong SAR, China*

[2]*Shenzhen Research Institute, The Chinese University of Hong Kong, Shenzhen 518057, China*

**Corresponding author: scchen@mae.cuhk.edu.hk; **corresponding author: yyam@mae.cuhk.edu.hk*

Received April 18, 2017; accepted June 16, 2017; posted online July 19, 2017

In this Letter, we present a high-speed volumetric imaging system based on structured illumination and an electrically tunable lens (ETL), where the ETL performs fast axial scanning at hundreds of Hz. In the system, a digital micro-mirror device (DMD) is utilized to rapidly generate structured images at the focal plane in synchronization with the axial scanning unit. The scanning characteristics of the ETL are investigated theoretically and experimentally. Imaging experiments on pollen samples are performed to verify the optical cross-sectioning and fast axial scanning capabilities. The results show that our system can perform fast axial scanning and three-dimensional (3D) imaging when paired with a high-speed camera, presenting an economic solution for advanced biological imaging applications.

OCIS codes: 180.6900, 180.2520, 220.1080.
doi: 10.3788/COL201715.090004.

In microscopy, optical cross-sectioning means the extraction of in-focus signals in the form of thin slides by the rejection of the out-of-focus signals or noises within a thick specimen[1]. Conventionally, this can be achieved by multi-photon microscopy[2,3], confocal microscopy[4], or structured illumination microscopy (SIM)[5,6]. However, multi-photon microscopy suffers from the high cost of laser sources; confocal microscopy has the issue of high phototoxicity. As point-scanning systems are typically slow compared with wide-field systems, SIM becomes a suitable and economic solution for a variety of high-speed biological imaging applications.

In SIM, three modulated images are obtained sequentially with a phase interval of $2\pi/3$ to reconstruct an optical cross-sectional image. Optical cross-sections are realized by the fact that high-frequency patterns attenuate rapidly when away from the focal region, and only the in-focus signals are modulated by the structured pattern. The imaging speed of SIM is limited by the speed of switching of structured patterns, which is conventionally achieved by mechanically scanning an optical grating[7,8]. Notably, this also results in motion/image artifacts and low optical sectioning efficiency[9]. More accurate phase shifts can be achieved by using a liquid-crystal-based spatial light modulator (LC-SLM) that has a speed of hundreds of Hz[10,11]. However, the LC-SLM is polarization-dependent and only modulates phases, which confines its application to a single excitation wavelength[12]. Compared with LC-SLMs, a digital micro-mirror device (DMD) is a cost-effective solution with substantially improved speed (4.2–32.5 kHz) and a broader spectral range[13–15].

Although the DMD-based SIM can rapidly generate two-dimensional (2D) optical cross-sections, a fast axial scanning method is still needed in order to realize high-speed volumetric imaging. Conventionally, volume imaging is achieved by axially scanning the specimen or objective lens to acquire images at different depths. However, the mechanical scanning process is slow and may introduce unwanted vibration and motion artifacts. These issues may be addressed by the application of an electrically tunable lens (ETL). An ETL is a transparent device whose optical power can be rapidly tuned by adjusting the drive current. Fast axial scanning has been successfully demonstrated in other optical systems by using ETLs with a speed of ~1 kHz[16–19].

In this Letter, we present a real-time three-dimensional (3D) fluorescent microscope system based on structured illumination and an ETL. In the system, a DMD is used to rapidly generate structured images, achieving high-speed 2D imaging. The ETL is used to perform fast axial scanning, realizing high-speed volumetric imaging. The speed of 3D imaging is only limited by the speed of cameras, i.e., tens of kHz. Figure 1 presents the optical configuration of the system. The light source is a light emitting diode (LED) (wavelength = 455 nm; M455L3, Thorlabs), which provides incoherent illumination free of speckles. Next, the light is collimated by a lens, L1 ($f = 30$ mm), and projected to the DMD (DLP4500, Texas Instruments). The DMD-modulated light is guided by a high-reflectivity mirror, M, and a collimating lens, L2 ($f = 100$ mm), to enter and fully fill the back aperture of the objective lens (Apo 40 × 1.15 NA, Nikon). Note that the system is aligned to satisfy Köhler illumination that has a uniform illumination at the front focal plane of the objective lens. The collimating lens, L2, and the objective lens together form a 4-f system that ensures

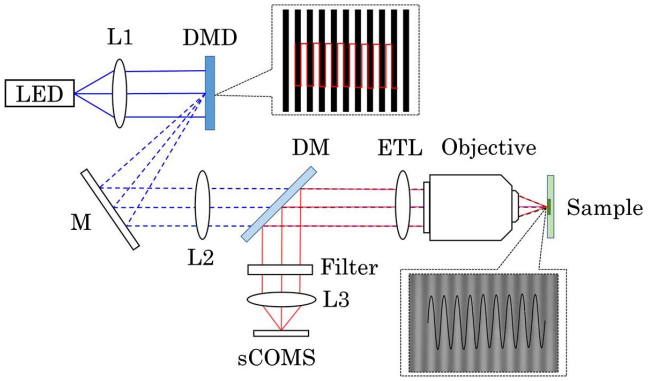

Fig. 1. Optical configuration of the DMD-based SIM system. L1, L2, and L3, collimating lenses; M, high-reflectivity mirror; DM, dichroic mirror.

the pattern on the DMD is precisely projected to the sample plane. The ETL (Speed: ~1 kHz; EL-10-30-Ci-VIS-LD-MV, Optotune) is placed 15 mm behind the objective lens to perform remote axial scanning. The ETL consists of a shape-changing lens and a pairing concave offset lens ($f_{\text{offset}} = -150$ mm) to achieve a tuning range from −1.5 diopter to +3.5 diopter during normal operation (i.e., drive current = 0–250 mA). The detection system shares the objective lens with the imaging system. The emissions from the specimen are separated from the excitation signals by a dichroic mirror (DMLP490, Thorlabs) and a long pass filter (BLP01-514 R-25, Semrock), and lastly focused onto a scientific complementary metal-oxide-semiconductor (sCMOS) camera (Zyla 4.2 PLUS, Andor) via a zoom lens, L3 (70–200 mm, Canon).

In this section, we investigate the optical performance of the SIM system. As shown in Fig. 2(a), first, an optical model that includes the ETL and objective lens is developed in ZEMAX, where the model of the objective lens is developed based on a Nikon patent[20]; the model of the ETL is obtained from Ref. [21]. In the model, the zero position refers to the original focal plane, i.e., the focal plane of the objective lens without the ETL. A positive focus shift means an increase in the working distance of the objective lens and vice versa. During normal ETL operation, the focal point can be shifted axially for ~300 μm. As can be observed in Fig. 2(b), the numerical aperture (NA) of the objective lens will vary when the focal point is scanned axially. It is worthwhile to note that the system resolution slightly decreases for both positive and negative focus shifts. This is expected, as the shifting of the focal plane will negatively affect the aberration correction capability of the objective lens[19]. Figures 2(b) and 2(c) present the NA variation versus different axial shift distance, as well as the corresponding lateral point spread functions (PSFs). Based on the analytic model of SIM[22], the axial resolution of our system is calculated to be 2.1 μm, where the magnification of the system is 20, and the period of the fringe pattern on the DMD is 64.8 μm. When scanned to the further distances (i.e., +50/−250 μm), the corresponding NA and axial resolution of the system are calculated to be 1.12/1.24 and 2.22/1.78 μm, respectively.

Next, we theoretically and experimentally study the relationship between the axial shift distance and the ETL drive current. This relationship is important in obtaining the precise depth information of individual optical sections for 3D reconstruction. In the experiments, the ETL scanning depth is determined by projecting high-frequency images to a high-reflectivity mirror driven by a precision z-stage; the scanning distance is identified for different ETL drive currents when the reflected images become in-focus and sharp on the camera. Figure 3(a) presents the results, where the theoretical values (solid line) match well with the experimental results (circles) throughout the ETL scanning range. Another side effect of using ETLs is the field magnification. Figure 3(b) plots the field magnification as a function of the ETL drive current, where the magnification is normalized to one at the zero position. The results show a 60% magnification variation when the focal point is scanned at 300 μm. In other words, the magnification varies ~2% for a 10 μm focus shift. Thus, for a small scanning range, e.g., tens of μm, the field magnification variation effect can be considered negligible. For long-range axial scanning, the results in

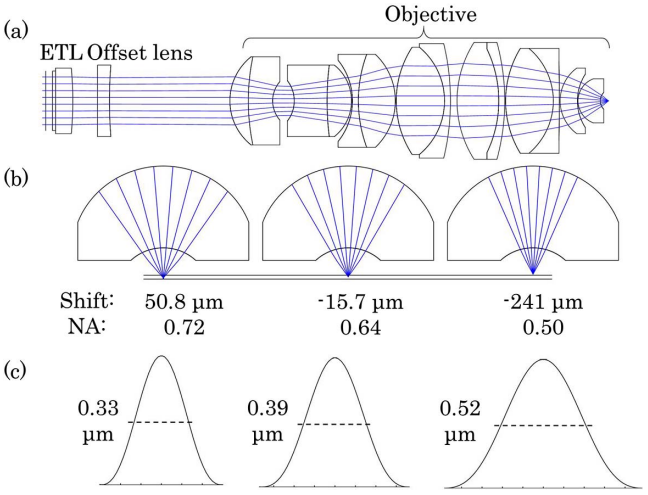

Fig. 2. (a) Optical models and ray-tracing analyses of the ETL and objective lens in ZEMAX, (b) NA variation during axial scanning, and (c) PSF variation during axial scanning.

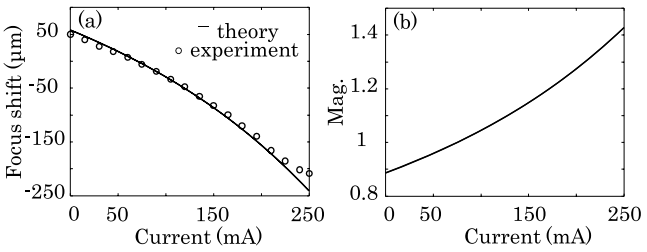

Fig. 3. (a) Relationship between the focus shift distance and ETL drive current, and (b) relationship between the field magnification and the ETL drive current.

Fig. 3 can be used to automatically correct the effect of field magnification.

In our system, the DMD is employed to rapidly generate structured patterns. A DMD is a 2D micro-mirror array capable of generating arbitrary binary patterns at high speed, i.e., 4.2–32.5 kHz. Figure 4(a) presents the binary fringe patterns programmed to the DMD at three different phases (pitch = 259.2 μm or 24 DMD pixels). The corresponding illumination patterns captured at the focal planes of the objective lens are presented in Fig. 4(b). Figure 4(c) presents the measured intensity profiles along the cut lines in Fig. 4(b). From the results, it can be observed that the fringes have sinusoidal profiles with accurate phase shifts, which forms a good foundation for the following computational processes.

To demonstrate the optical cross-sectioning capability of our SIM system, we compare images obtained by the SIM and a wide-field microscope, as shown in Fig. 5. From Fig. 5(a), it can be clearly observed that only a thin section of the pollens are imaged, and the out-of-focus emissions have been removed, indicating good optical cross-sectioning capability. On the other hand, the wide-field image looks blurry. The results in Fig. 5 are obtained based on[5]

$$I_s = \frac{\sqrt{2}}{3}\sqrt{(I_1 - I_2)^2 + (I_1 - I_3)^2 + (I_2 - I_3)^2}, \quad (1)$$

where I_1, I_2, and I_3 are the intensities of the three phase-modulated images with a phase interval of $2\pi/3$, and I_s is the reconstructed image with the structured patterns removed and the out-of-focus signals rejected.

Lastly, we axially scan the pollen sample via both the ETL and a precision z-stage and compare the image quality. Figures 6(a)–6(d) and 6(e)–6(h) present the 3D imaging results of pollen grain samples, scanned by the ETL and precision z-stage, respectively. Images of four selected depths, i.e., 12, 9, 7, and 5 μm, are presented, where the images of the same depths are grouped in the same row, showing indistinguishable quality and resolution throughout the scanning range. The field magnification effect is also negligible (~2%) in Fig. 6. To achieve high-speed imaging, the ETL, DMD, and camera are synchronized and controlled via a custom-developed LabVIEW program. The imaging speed of the SIM system is limited by the speed of the camera. As the speed of our sCMOS camera can operate up to 1600 Hz in the external trigger mode, real-time 3D imaging may be realized. Note that the

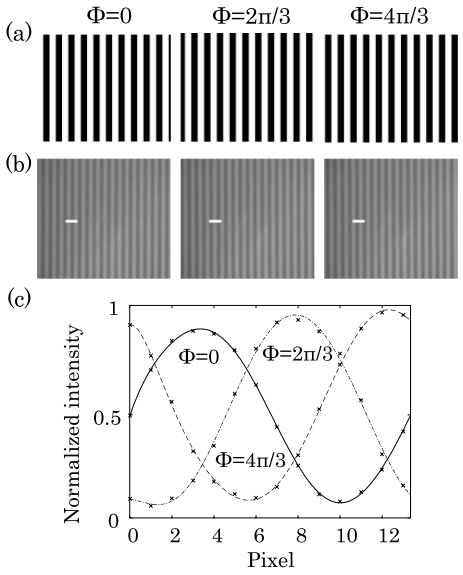

Fig. 4. Generation of phase-shifted sinusoidal fringes using a DMD: (a) binary patterns programmed to the DMD at three different phases; (b) corresponding illumination patterns captured at the objective focal plane; (c) measured intensity profiles of the illumination patterns along the cut-lines in (b) for the three phases, i.e., $\Phi = 0$, $2\pi/3$, and $4\pi/3$.

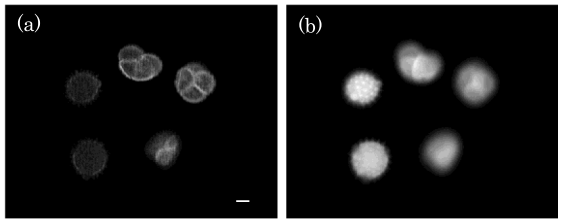

Fig. 5. (a) Pollen imaging results from our SIM system versus (b) a regular wide-field microscope. Scalar bar = 10 μm.

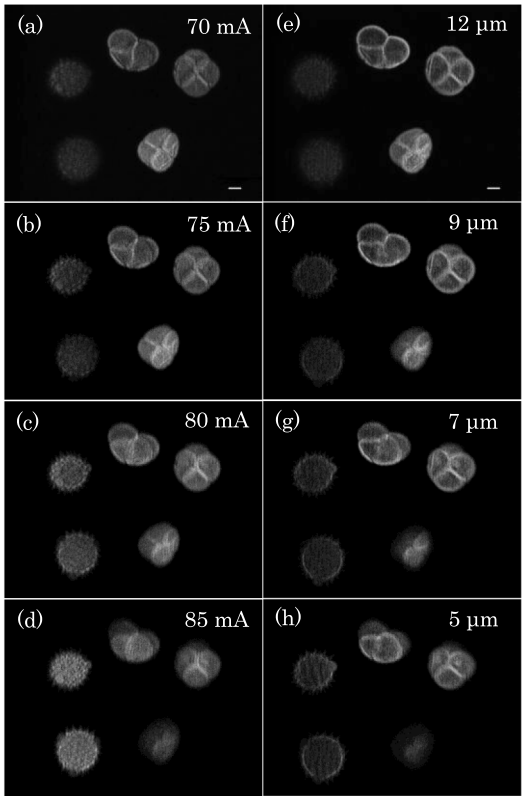

Fig. 6. (a)–(d) Images obtained by the ETL; (e)–(h) images obtained by the precision z-stage. Images of the same depths are grouped in the same row. Scalar bar = 10 μm.

imaging speed of our SIM system can be substantially improved with a high-speed camera, e.g., FASTCAM SA-Z camera (Photron), which operates at 21000 fps with full resolution[23]. With this camera, the SIM may image at a speed of 7000 Hz, realizing ultrafast 3D imaging.

In conclusion, we present a low-cost, high-speed SIM system based on a DMD and ETL for 3D imaging. The wide-field detection of SIM enables fast imaging acquisition, where the speed is only limited by the camera. Accordingly, real-time 3D imaging may be realized via a high-speed camera and fast axial scanner, i.e., ETL. The performance of the SIM system is theoretically and experimentally investigated, including the NA variation and field magnification at different scanning depths. 3D imaging is performed on pollen samples, showing indistinguishable quality and resolution compared with a mechanical scanner throughout the scanning range. The system may be used to image high-speed biological events, generating impact for biological studies.

This work was supported by the National Natural Science Foundation of China (NSFC), General Program (No. 51375415) and the Development of a Flexure-based Optical Scanning System and a Multimodal Nonlinear Endomicroscope for in vivo Biological Studies, as well as the HKSAR Research Grants Council (RGC) General Research Fund (CUHK 14202815).

References

1. J. Mertz, Nat. Methods **8**, 811 (2011).
2. W. Denk, J. H. Strickler, and W. W. Webb, Science **248**, 73 (1990).
3. F. Helmchen and W. Denk, Nat. Methods **2**, 932 (2005).
4. R. H. Webb, Rep. Prog. Phys. **59**, 427 (1996).
5. M. A. A. Neil, R. Juskaitis, and T. Wilson, Opt. Lett. **22**, 1905 (1997).
6. M. Saxena, E. Gangadhar, and S. S. Gorthi, Adv. Opt. Photon. **7**, 241 (2015).
7. Y. Markaki, D. Smeets, S. Fiedler, V. J. Schmid, L. Schermelleh, and T. Cremer, Bio. Essays **34**, 5 (2012).
8. T. Hinsdale, B. H. Malik, C. Olsovsky, J. A. Jo, and K. C. Maitland, Opt. Lett. **40**, 4943 (2015).
9. H. W. Lu-Walther, M. Kielhorn, R. Förster, A. Jost, K. Wicker, and R. Heintzmann, Methods Appl. Fluoresc. **3**, 014001 (2015).
10. P. Kner, B. B. Chhun, E. R. Griffis, L. Winoto, and M. G. Gustafsson, Nat. Methods **6**, 339 (2009).
11. B. J. Chang, L. J. Chou, Y. C. Chang, and S. Y. Chiang, Opt. Express **17**, 17 (2009).
12. L. Shao, P. Kner, E. H. Rego, and M. G. Gustafsson, Nat. Methods **8**, 1044 (2011).
13. A. G. York, S. H. Parekh, D. Dalle Nogare, R. S. Fischer, K. Temprine, M. Mione, A. B. Chitnis, C. A. Combs, and H. Shroff, Nat. Methods **9**, 749 (2012).
14. J. Cheng, C. Gu, D. Zhang, D. Wang, and S. C. Chen, Opt. Lett. **41**, 7 (2016).
15. D. Xu, T. Jiang, A. Li, B. Hu, Z. Feng, H. Gong, S. Zeng, and Q. Luo, J. Biomed. Opt. **18**, 6 (2013).
16. H. J. Jeong, H. Yoo, and D. Gweon, Opt. Express **24**, 4 (2016).
17. F. O. Fahrbach, F. F. Voigt, B. Schmid, F. Helmchen, and J. Huisken, Opt. Express **21**, 18 (2013).
18. B. F. Grewe, F. F. Voigt, M. van't Hoff, and F. Helmchen, Biomed. Opt. Express **2**, 2035 (2011).
19. J. Jiang, D. Zhang, S. Walker, C. Gu, Y. Ke, W. H. Yung, and S. C. Chen, Opt. Express **23**, 19 (2015).
20. K. Yamaguchi, "Immersion microscope objective lens," U.S. patent 6,519,092 (February 11, 2003).
21. https://www.optotune.com/.
22. P. A. Stokseth, J. Opt. Soc. Am. **59**, 1314 (1969).
23. https://photron.com/high-speed/cameras/fastcam-sa-z/.